12-1-2022

Wavenumbers 3 and 4 Quasi 2-day Wave Activities Observed by Multiple Meteor Radars in the Two Hemispheres During Austral Summer

Hao Cheng
Wuhan University, Ministry of Education

Kai Ming Huang
Wuhan University, Ministry of Education

Alan Z. Liu
Embry Riddle Aeronautical University, liuz2@erau.edu

Shao Dong Zhang
Ministry of Education

Chun Ming Huang
Wuhan University, Ministry of Education

See next page for additional authors

JGR Space Physics

RESEARCH ARTICLE
10.1029/2022JA030501

Wavenumbers 3 and 4 Quasi 2-day Wave Activities Observed by Multiple Meteor Radars in the Two Hemispheres During Austral Summer

Hao Cheng[1,2], Kai Ming Huang[1,2], Alan Z. Liu[3], Shao Dong Zhang[2], Chun Ming Huang[1,2], and Yun Gong[1,2]

[1]School of Electronic Information, Wuhan University, Wuhan, China, [2]Key Laboratory of Geospace Environment and Geodesy, Ministry of Education, Wuhan, China, [3]Department of Physical Science, Embry Riddle Aeronautical University, Daytona Beach, FL, USA

Key Points:

- W3 and W4 dominate the first and second bursts of quasi 2-day wave respectively and transition from W3 to W4 is completed around the end of January
- W3 and W4 have nearly same dominant period and vertical wavelengths and similar latitude and altitude distributions in two hemispheres
- W3 and W4 originate from instabilities of summer easterly jets in the lower mesosphere and stratopause region

Correspondence to:
K. M. Huang,
hkm@whu.edu.cn

Citation:
Cheng, H., Huang, K. M., Liu, A. Z., Zhang, S. D., Huang, C. M., & Gong, Y. (2022). Wavenumbers 3 and 4 quasi 2-day wave activities observed by multiple meteor radars in the two hemispheres during austral summer. *Journal of Geophysical Research: Space Physics*, *127*, e2022JA030501. https://doi.org/10.1029/2022JA030501

Received 26 MAR 2022
Accepted 1 DEC 2022

Abstract Combining observations from three meteor radars in the Northern Hemisphere (NH) and a meteor radar in the Southern Hemisphere (SH) and reanalysis data, we present successive wavenumbers 3 and 4 (W3 and W4) quasi 2 day wave activities in austral summer. In the mesosphere and lower thermosphere, the wave exhibits two burst activities. The W3 dominates the first burst, while the W4 is the predominate mode in the second burst. The mode transition arises in the late January and is completed around the end of January. The W3 and W4 have the nearly same dominate period of about 46 hr and vertical wavelengths of 110 km in the SH and about 55–65 km in the NH, and the similar latitude and altitude distributions in the zonal and meridional winds and temperature, except stronger magnitude and farther extension in the NH for the W3. The analysis indicates that the unstable regions of the summer jets in the lower mesosphere and stratopause region have the boundaries which toward lower latitudes are largely consistent with the critical layers, and Eliassen-Palm (EP) fluxes of the W3 and W4 increase rapidly near the unstable regions. This demonstrates that both the W3 and W4 originate from the jet instabilities. Nevertheless, the EP flux of the W3 shows a stronger transfer across the hemispheres than that of the W4. The W3 and W4 have the same period and vertical scale, which is different from previous reports.

1. Introduction

The inherent ability of the atmosphere to support wave motions is one of its most important dynamical properties. Planetary waves (PWs) resulting from northward potential vorticity gradient are a global scale atmospheric perturbation, which plays a vital role in driving stratospheric circulation and transporting momentum and energy across the hemispheres in the mesosphere and lower thermosphere (MLT) region (Andrews et al., 1987). Quasi 2-day wave (QTDW) is a prominent PW in the MLT due to the very large amplitude in its outbreak periods. In recent decades, the general features of QTDW in the MLT have been extensively studied by radar (Fritts et al., 2019; Gaikwad et al., 2019; K. M. Huang, Liu, et al., 2013; Jacobi et al., 1997; Lima et al., 2004; Pancheva et al., 2004; Rao et al., 2017; Suresh Babu et al., 2011) and satellite (Ern et al., 2013; Forbes & Moudden, 2012; Gu et al., 2013; Y. Y. Huang, Zhang, et al., 2013; Limpasuvan & Wu, 2009) observations. These studies revealed that the QTDW is basically a summertime phenomenon in both the hemispheres, maximized usually at middle to low latitudes after solstices, with much larger amplitudes in the southern hemisphere (SH) than in the northern hemisphere (NH). In the SH, The QTDW is observed to be mostly a westward propagating zonal wavenumber 3 (W3) mode, with periods close to 48 hr, while in the NH, the wave is often a mixture of W2, W3 and W4, with a period range of 42–56 hr (Craig et al., 1980; Fritts et al., 1999; Malinga & Ruohoniemi, 2007) possibly due to the superposition of different zonal wavenumber components (Thayaparan et al., 1997). Recently, two meteor radar observations at Mohe (122°E, 54°N) and northern Germany (13°E, 53°N) reported that the W3, W4 and E3 are the active QTDW modes at mid latitude in the NH during the summer (He, Forbes, et al., 2021), indicating a possibly seasonal and latitudinal dependence of the dominant modes. Besides, the lifetime of the NH wave event is typically more than a month, whereas the duration of the SH wave event is more like pulses (Fritts et al., 1999; Gu et al., 2013; Harris & Vincent, 1993; Thayaparan et al., 1997).

In the MLT, the vertical wavelength of QTDW is generally rather long (>50 km) in the two hemispheres, and the maximum amplitude arises at heights of 75–100 km (Harris & Vincent, 1993; Lilienthal & Jacobi, 2015; Rao et al., 2017). The meridional wind amplitude tends to be larger than the zonal wind amplitude at mid-latitudes

(Fritts et al., 2019), which is different from other period PWs generally with a stronger magnitude in the zonal wind. In the upper mesosphere, the amplitudes in the meridional and zonal winds can reach up to about 50 and 30 ms^{-1}, respectively, and the amplitude in the temperature may be up to about 11 K (Limpasuvan & Wu, 2003; Palo et al., 2007). The QTDW in the horizontal winds and temperature is most pronounced at mid latitudes in summer, and is also able to penetrate from the summer hemisphere into the winter hemisphere (Tunbridge et al., 2011).

In theoretical and modeling studies, two main mechanisms are proposed to explain the occurrence of QTDW in the middle atmosphere. Salby (1981, 1984) considered the QTDW as a manifestation of the Rossby-gravity normal mode driven chiefly by flow over orography and thermal contrast, which is largely influenced by the mean fields. By using a linearized spectral mode to carry out a series of numerical experiments for January conditions, Hagan et al. (1993) provided the evidence that the QTDW in the upper mesosphere may be a signature of W3 mixed Rossby-gravity mode, and the W3 is sensitive to the zonal mean wind in the MLT. In contrast, Plumb (1983) and Pfister (1985) suggested that the seasonal variability of QTDW is related to baroclinic instability of the easterly jet in the summer mesosphere. Based on a two-dimensional stability analysis, the spectral peaks of the baroclinically unstable growth wave components were at zonal wavenumbers 2–4 with periods of 1.4–3 days for a variety of basic state flows, and the unstable waves were generally trapped between 40° and 60° latitudes (Pfister, 1985). Nevertheless, observations indicated that the QTDW has a more global structure (Fritts et al., 2019; Moudden & Forbes, 2014; Pancheva et al., 2018; Riggin et al., 2004).

By combining the two mechanisms, Salby and Callaghan (2001) suggested that the wave activity generated by instabilities disperses globally into the Rossby-gravity modal structure. Meanwhile, they found that the W3 is in phase in the meridional wind between the two hemispheres, but is out of phase in the zonal wind and temperature between the hemispheres (Tsuda et al., 1988). The W3 amplification is sensitive to the zonal mean background, and the changes of the mean flow could sharply alter its growth rate, but have little effect on its eigen period and structure. Some satellite observation (Garcia et al., 2005; Limpasuvan & Wu, 2003) and global modeling studies (McCormack et al., 2009; Norton & Thuburn, 1996; Richter et al., 2008; Schröder & Schmitz, 2004; Yue et al., 2012) indicated that the QTDW is primarily a global normal mode wave arising from localized baroclinic or barotropic instabilities, that is, negative meridional gradient of potential vorticity. In addition, nonlinear interactions between the diurnal tide and the QTDW could cause the amplification of QTDW (Chang et al., 2011; K. M. Huang, Liu, et al., 2013; Jacobi et al., 1998; Palo et al., 1999; Walterscheid & Vincent, 1996).

Using observations from a network of 15 radars situated in the NH, Pancheva et al. (2004) reported the simultaneous occurrence of the W2, W3 and W4 during the summer of 1999, with the periods of about 53–56, 48–50, and 42–43 hr, respectively. They proposed the possibility that the W2 and W4 could be generated by the non-linear interactions between the W3 and the 14–17 day PW. In the thermosphere ionosphere mesosphere energetics dynamics/sounding of the atmosphere using broadband emission radiometry (TIMED/SABER) measurement, the W3 has a dominate period of about 51 hr and an average vertical wavelength of about 85 km in the MLT, which are larger than the corresponding period and wavelength of about 48.8 hr and 70 km of the W4 (Y. Y. Huang, Zhang, et al., 2013), respectively. Whereas, in the Aura/microwave limb sounder observation, the W3 has an average period of about 50 hr in the NH and about 48 hr in the SH, and the W4 has a larger average period of about 54 hr in both the two hemispheres (Pancheva et al., 2018). In numerical investigation from a global circulation model, transition from a predominant W3 to a W4 on the equator typically occurs in February and August (Norton & Thuburn, 1996), and satellite and radar observations showed a case of the transition from a W3 to a W4 in August (Riggin et al., 2004). Nevertheless, the associated dynamics is not analyzed in detail. Hence, the dominant period, vertical wavelength, latitudinal distribution and possible origin of the different QTDW modes and their transition still need to require constant attention by observational and modeling studies.

In this paper, combining multiple meteor radar observations in both the hemispheres and reanalysis data, we present successive burst W3 and W4 QTDW activities during the austral summer of 2011. The temporal and spatial scales, propagation features and latitudinal structures of the W3 and W4 are compared, and their possible origin and transition are discussed. In the next Section, the meteor radars and datasets utilized are described in brief. In Section 3, we analyze the temporal and spatial evolution of the observed QTDW components in detail, and attempt to identify the possible excitation and amplification of the W3 and W4 in Section 4. Finally, Section 5 provides a summary.

2. Data Sets

The horizontal winds measured by four meteor radars arranged approximately along the 115°E–65°W meridian circle from mid latitude of the SH to mid latitude of the NH and the wind and temperature data from the Modern-Era Retrospective Analysis for Research and Applications (MERRA) for 60 days from 1 January 2011 to 1 March 2011 are used in present study.

The three meteor radars are situated at Beijing (40.3°N, 116.2°E), Wuhan (30.5°N, 114.6°E), and Sanya (18.3°N, 109.6°E) in China, established by the Institute of Geology and Geophysics, Chinese Academy of Sciences. These meteor radars can provide horizontal winds in the height range of 78–100 km with a temporal resolution of 1 hr and a vertical resolution of 2 km. The fourth meteor radar is located at Andes (30.3°S, 70.7°W) in Cerro Pachón, Chile, which can obtain the hourly vertical profiles of horizontal winds sampled at a 1 km interval in the height range of 80–100 km. All of these radars are all-sky interferometric meteor radar, which record the radial velocity of individual meteor trails, and then combine these radial velocities in an all-sky manner to determine the zonal and meridional winds (Hocking et al., 2001). The detailed technical specifications of the four radar systems can be found in early works (Cheng et al., 2021; Franke et al., 2005; K. M. Huang et al., 2019; Y. Yu et al., 2015).

The number of meteor counts detected by the radar showed a strong dependence on altitude, with an approximate Gaussian distribution centered at about 88–90 km, thus the uncertainty of wind measurement is small with typical values of 3–4 ms^{-1} around 88–90 km (Franke et al., 2005; Hocking et al., 2001; X. S. Huang et al., 2022). As the height goes up and down, the detection number of meteors reduces, and then the statistical wind uncertainties increase gradually, and may sometimes exceed 10 ms^{-1} at the heights of 80 and 100 km. Even so, the comparison indicated a good consistency of the zonal and meridional winds at 80–100 km between the meteor radar and the narrowband Sodium Doppler lidar observations (Franke et al., 2005). Hence, the meteor radar observations are suitable for investigating the dynamical process of large-scale PW activity.

The reanalysis data can help us to identify the zonal wavenumber of QTDW. The version 2 of MERRA (MERRA2) is a global atmospheric reanalysis produced by the Goddard Earth Sciences Data and Information Services Center of the National Aeronautics and Space Administration, which is obtained from the online archive at https://disc.gsfc.nasa.gov/datasets. The MERRA2 reanalysis data is distributed on 0.5° × 0.625° latitude-longitude grids for 72 pressure levels from the ground up to 0.01 hPa with a time step of 6 hr (Gelaro et al., 2017). The 0.01 hPa level corresponds to a height of about 80 km, thus the two data sets have a fine connection in height. Nevertheless, owing to non uniformly spaced levels in the reanalysis data, we need to bear in mind that the height difference between two adjacent pressure levels increases gradually from about 0.1 km on the ground to about 5 km at the top level, and some variations and processes in the upper stratosphere and mesosphere may not be clearly represented in the reanalysis data (Manney et al., 2008). All data utilized in the paper are unified to the universal time (UT), and 1 January 2011 is referred to as day 1 for the period of 60 days.

3. W3 and W4 QTDW Activities

3.1. QTDW Activity in MLT

Figure 1 shows the daily mean zonal (positive eastward) and meridional (positive northward) winds observed by the meteor radars at the four stations from 1 January 2011 to 1 March 2011. There is a lack observation at Sanya for the first three days. The strong quasi 2-day oscillation in both the zonal and meridional winds can be clearly seen from Figure 1, especially in the meridional winds at Andes and Sanya, and the magnitude of the QTDW gradually decreases from Andes at mid latitude of the SH to Beijing at mid latitude of the NH.

In order to investigate the temporal behavior of the QTDW, we carry out a wavelet transform on the zonal and meridional winds at 90 km observed by the radars since the missing data is minimal at this height due to the high meteor acceptance rate. The percentage of the missing data is only about 3.6%, 3.7%, 6.7%, and 0.4% at Andes, Sanya (excluding lack observation in the first 3 days), Wuhan, and Beijing, respectively, and the missing data are replaced with linear interpolation. Wavelet used here is composed of a Morlet wavelet function of nondimensional wavenumber 6, which is extensively applied to decompose the time-varying wave components from a temporal series of atmospheric observations in the MLT (Cheng et al., 2021; K. M. Huang et al., 2015; Pancheva et al., 2018; F. R. Yu et al., 2019). Figure 2 presents the wavelet spectra of the zonal and meridional winds at 90 km in the period range of 30–72 hr. At the four stations, the spectral amplitude enhancement of QTDW can

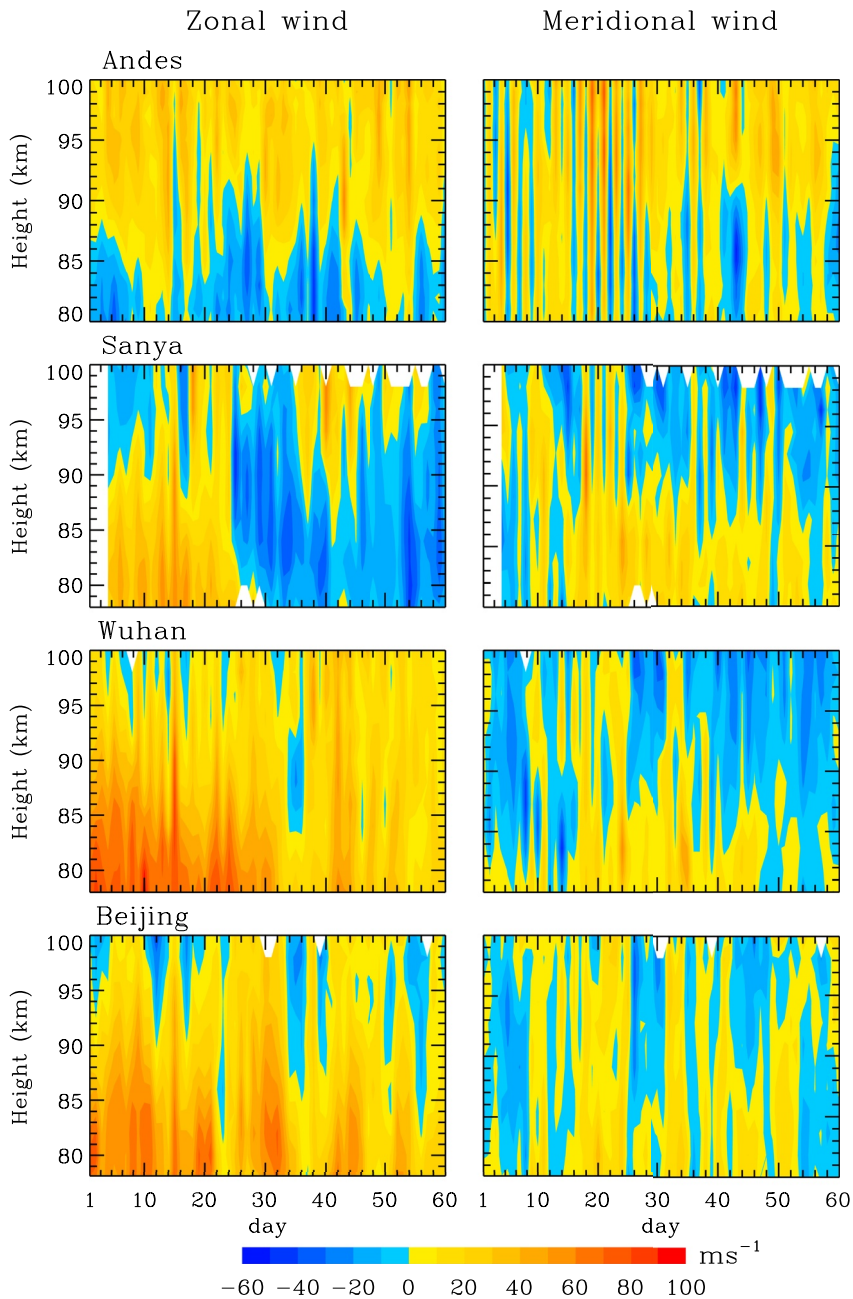

Figure 1. Daily mean zonal and meridional winds observed by meteor radars at four stations from 1 January 2011 to 1 March 2011. The left and right columns denote the zonal and meridional winds, respectively. 1 January 2011 is marked as day 1 for the period of 60 days.

be noted in the meridional and zonal winds, and in general, the spectral peaks are at 45–47 hr slightly less than 48 hr in both the two hemispheres. The spectral intensity is obviously stronger in the meridional wind relative to in the zonal wind. At Andes, the maximum spectral amplitude is as large as about 80 ms^{-1} in the meridional wind in days 20–23, and about 40 ms^{-1} in the zonal wind, which are in good agreement with the zonal and meridional wind amplitudes as high as about 40 and 80 ms^{-1} in the radar observations at mid and low latitudes of the SH on 20–25 January 2015 (Fritts et al., 2019). As latitude changes, the spectral magnitude is gradually weakened from mid latitude of the SH to mid latitude of the NH, which is consistent with the QTDW variation shown in Figure 1.

In addition, it is noted from Figure 2 that the time dependence characteristics of the QTDW show some similarity in the meridional wind. There are two bursts on the wave activity at Andes, Sanya and Wuhan. The first burst

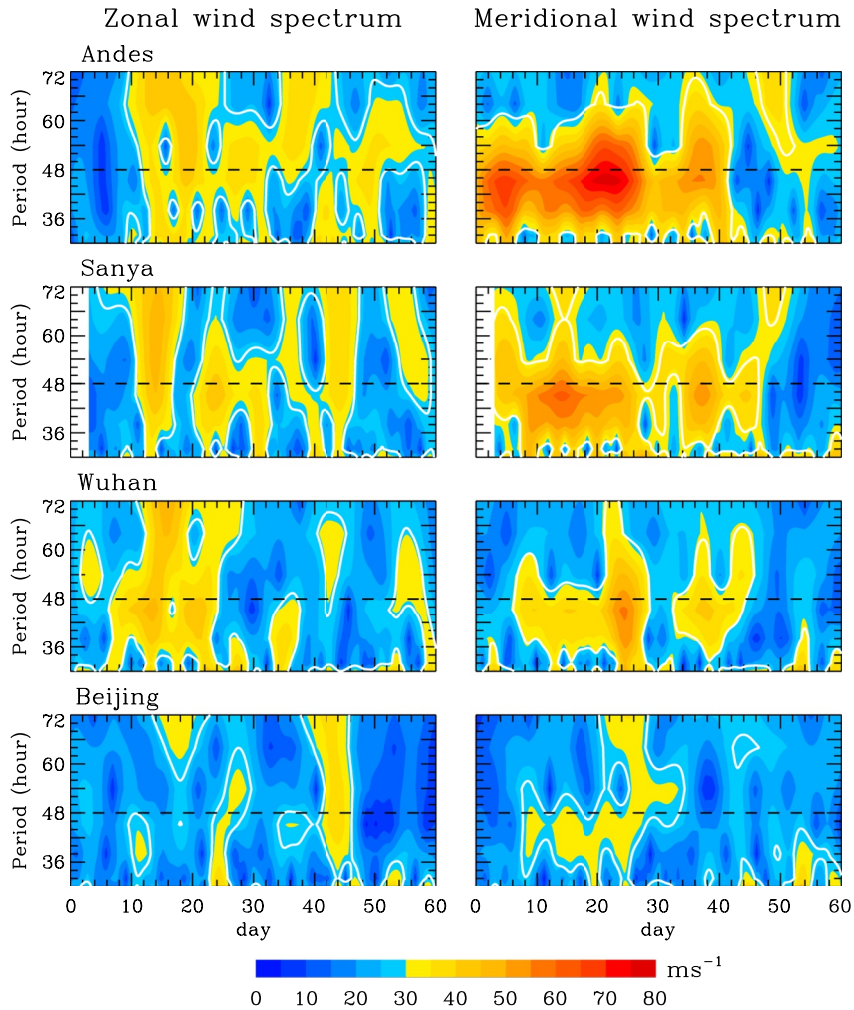

Figure 2. Wavelet spectra of zonal and meridional winds at 90 km observed by meteor radars at four stations. The left and right columns denote the spectra of the zonal and meridional winds, respectively. The dashed horizontal line corresponds to a period of 48 hr, and the white curves represent the confidence level of 95%.

occurs at all the four stations before about day 30, while the second one seems not to occur obviously at Beijing after day 30 due probably to the decrease of the wave magnitudes with increasing latitude in the NH. The two wave bursts are separated from each other at Wuhan, and can also be distinguished from each other at Sanya and Andes. The similar features of the wave activities may be seen in the zonal wind but with slightly more intermittent. In view of the above, our analysis will mainly focus on the QTDW activities in the meridional winds.

By using the meridional winds from the radar and MERRA2 reanalysis data at the four radar stations, we extract the QTDW through a bandpass filter to examine the wave activities from the lower atmosphere to the MLT. The bandpass periods of 42–56 hr are chosen based on the wavelet spectra in Figure 2. Figure 3 presents the filtered QTDW in the meridional wind over the four stations. In Figure 3, the corresponding altitude in the reanalysis data is derived from logarithmic pressure-height formula under a scale height of 7 km. The filtered QTDWs around 80 km show a good consistency of wave amplitudes and phases between the radar observations and the reanalysis data, indicating the reliability of these two datasets. Nevertheless, there are also a few small differences between the two data sets, for instance, the amplitude at 80 km at Andes is significantly larger in the radar measurements than in the reanalysis data, and similarly, some discrepancies in the upper stratosphere and mesosphere between the assimilated reanalysis data and the observations were also noticed in early study (Manney et al., 2008). It is interesting that in Figure 3, the QTDW is gradually strengthened from about 48 to 80 km, but does not evidently appear below 48 km. Meanwhile, at all the stations, the wave phase progresses downward, indicating the upward propagation of the QTDW from the upper stratosphere to the MLT. This implies that the

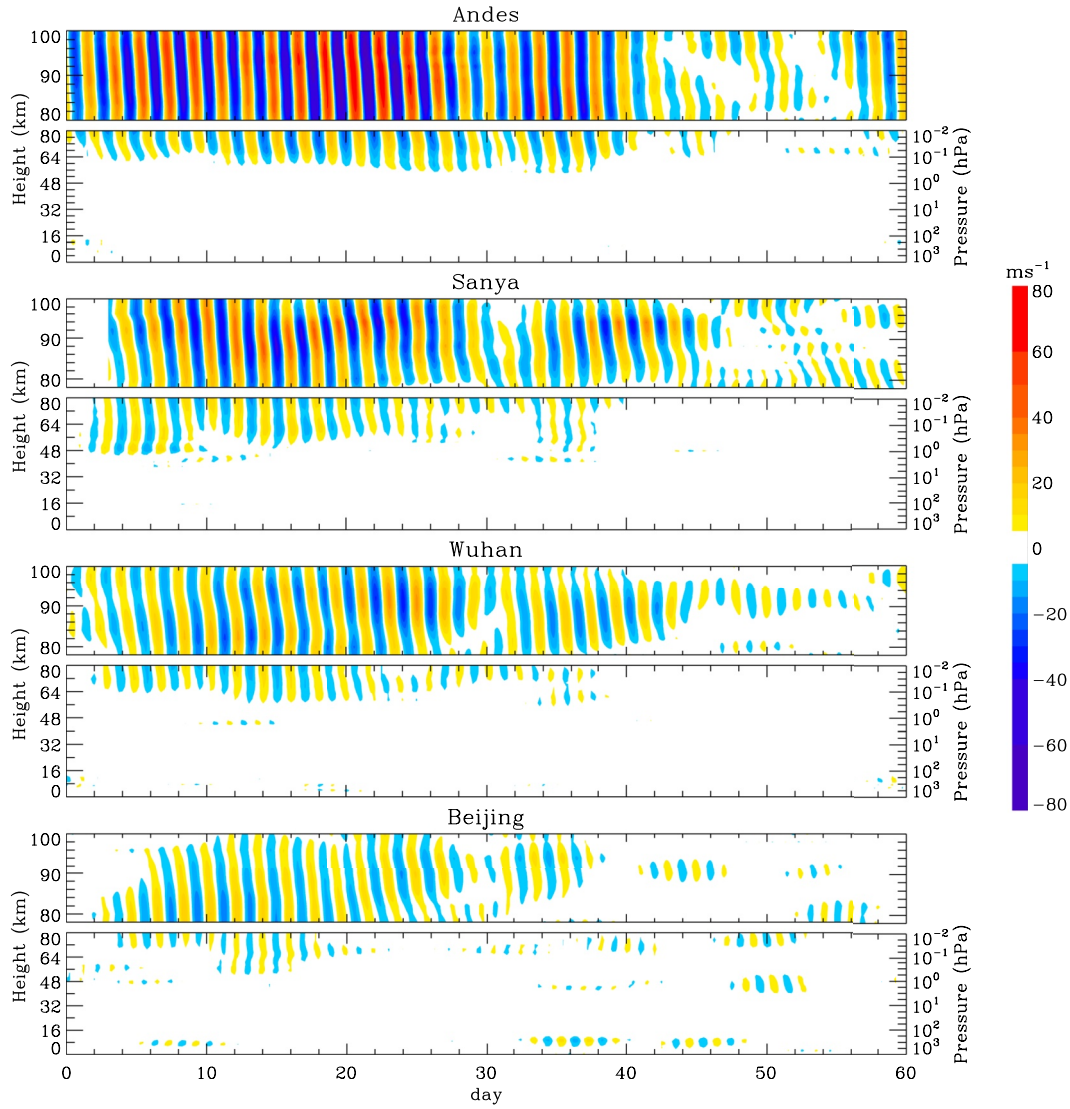

Figure 3. Band pass filtered quasi 2-day wave in meridional wind from radar observations and Modern-Era Retrospective Analysis for Research and Application version 2 reanalysis data at four stations. For the reanalysis data, the pressure level and corresponding height are marked on the right and left vertical axes, respectively.

excitation and amplification of the QTDW probably take place from the stratopause region to the lower mesosphere. The two breakouts of the QTDW and their transition around day 30 can clearly be noted in Figure 3. The first burst is stronger and lasts longer than the second one.

3.2. W3 and W4 Modes

By means of the MERRA2 reanalysis data, we determine whether the two outbreak QTDW events are a same wave mode. Now that the two QTDW events are the most intense at mid latitudes in the SH, we select the reanalysis zonal and meridional winds and temperature at the 0.01 hPa level over 40°S in days 13–22 and days 32–41 to perform a Fast Fourier Transform, respectively. Figure 4 depicts the frequency-wavenumber spectra of the meridional wind, zonal wind and temperature from the reanalysis data. The negative sign before wavenumber in Figure 4 denotes the westward wave propagation. The standard deviations for the zonal and meridional winds and temperature are 16.7 ms^{-1}, 19.4 ms^{-1}, and 6.9 K in days 13–22, and 10.9 ms^{-1}, 14.1 ms^{-1}, and 5.1 K in days 32–41, respectively. The weak components with the spectral peaks less than the minimum contours are not presented. In all the zonal and meridional winds and temperature, the zonal wavenumber is −3 in the first QTDW

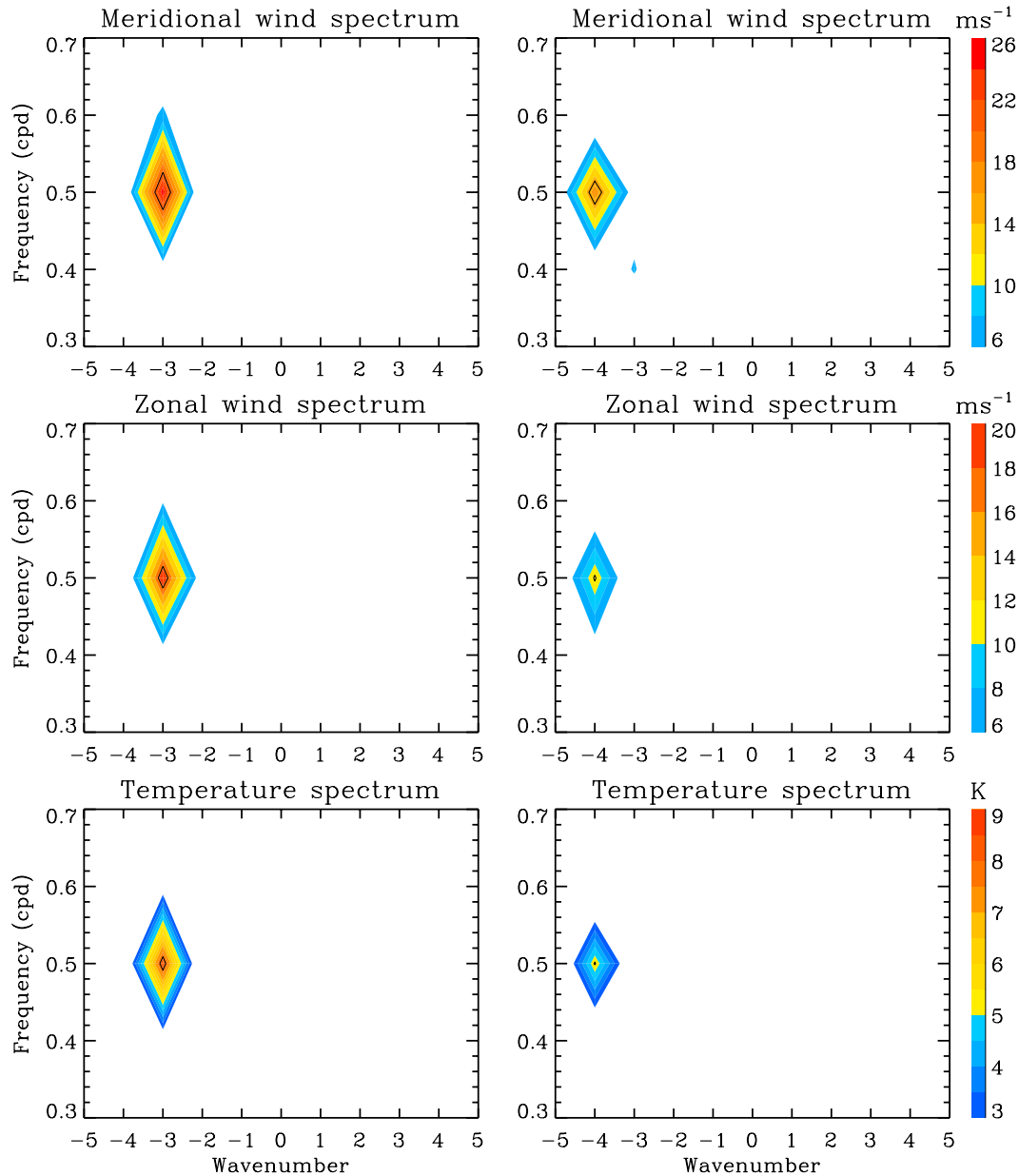

Figure 4. Frequency-wavenumber spectra of zonal and meridional winds and temperature at 0.01 hPa over 40°S during days 13–22 and days 32–41 from Modern-Era Retrospective Analysis for Research and Application version 2 reanalysis data. The left and right columns represent the two-dimensional spectra in days 13–22 and days 32–41, respectively, and the negative wavenumber denotes the westward wave propagation. The black contours on the left (right) column represent the standard deviations of 16.7 (10.9) ms^{-1}, 19.4 (14.1) ms^{-1}, and 6.9 (5.1) K in the zonal wind, meridional wind and temperature during days 13–22 (32–41), respectively.

event, but −4 in the second one, and there are no other strong QTDW modes during the 60-day duration, such as W2. In different SH summers, other modes, such as W2, E1, E2, and E3, may exhibit significant activities (Fritts et al., 2019; Harris & Vincent, 1993; He, Chau, et al., 2021; He, Forbes, et al., 2021), which implies that the QTDW bursts are the generality in the SH summer but the modes might slightly change from summer to summer. The spectral peaks of 25.3 ms^{-1}, 19.8 ms^{-1}, and 8.4 K of the W3 in the meridional wind, zonal wind and temperature are larger than those of 17.4 ms^{-1}, 11.7 ms^{-1}, and 5.5 K of the W4, which is consistent with the results in Figures 2 and 3. In particular, during the second burst event after day 30, there is not a significant spectral peak at westward wavenumber 3, thus the W3 and W4 modes dominate the first and second outbreak QTDW perturbations, respectively, and the transition from the dominant W3 to the W4 is completed around about day 30.

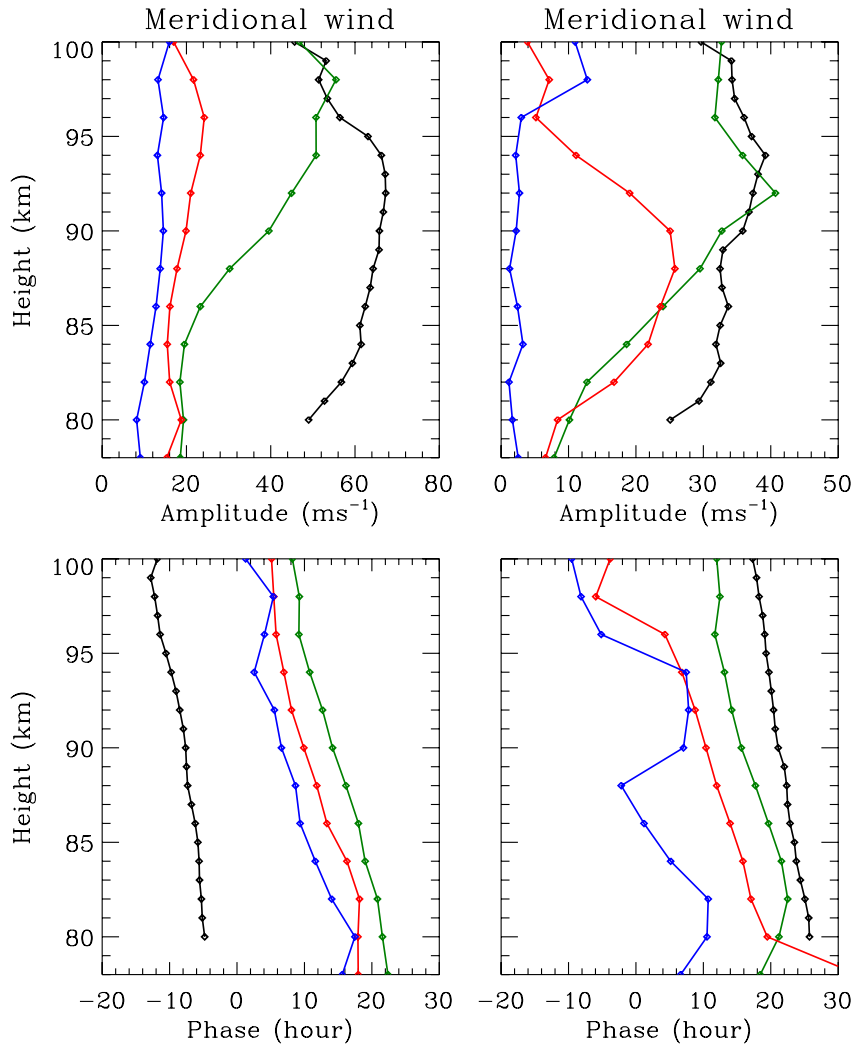

Figure 5. Fitted amplitudes and phases of W3 and W4 in meridional wind during days 17–22 and days 36–41 from radar observations. The upper and lower rows denote the fitted amplitudes and phases, and the left and right columns represent the fitted results in days 17–22 and days 36–41, respectively. The black, green, red and blue curves denote the results at Andes, Sanya, Wuhan, and Beijing, respectively.

Based on the phase variation with height, we estimate the vertical scales of the W3 and W4 in the MLT of the two hemispheres from the radar observations. A sinusoidal wave fit is performed on the meridional wind in days 17–22 and days 36–41, respectively, and the fitting period is chosen as 46 hr from the wavelet spectra in Figure 2. Figure 5 presents the fitted amplitudes and phases of the W3 and W4 in the meridional wind. The fitted phase is expressed by the time of the maximum wave perturbation (K. M. Huang et al., 2015). The fitted amplitudes of both the W3 and W4 show a decrease trend from mid latitude of the SH to mid latitude of the NH. At Andes, the fitted amplitude is very strong, and the fitted phase propagates steadily downward, while at Beijing, the fitted phase progresses downward with large fluctuations, which is probably caused by interference with the fitted phase, due to the rather weak wave magnitude. At the three stations in the NH, the wave phases of the W3 and W4 tend to lead in turn from low latitude to mid latitude. For Rossby modes with westward phase propagation, group velocity is in opposite to phase velocity in the meridional direction, similar to that in the vertical direction. The southward phase progression implies the northward propagation of both the W3 and W4, which indicates that the two QTDW components may originate from the SH. By further linearly fitting on these wave phases, the vertical wavelengths of the W3 (W4) are estimated to be about 67 (57), 65 (52), 65 (63), and 111 (110) km at Beijing, Wuhan, Sanya and Andes. At the three stations of the NH, the vertical scales are similar to each other, but are smaller than at the Andes station of the SH, which is qualitatively consistent with the result of the vertical

wavelength in the SH being longer than in the NH (Y. Y. Huang, Zhang, et al., 2013). Therefore, it is interesting that the W3 and W4 have not only the same propagation directions but also the similar dominant period and vertical wavelength in the two hemispheres, which is different from early observations (Fritts et al., 2019; Pancheva et al., 2004).

3.3. Global Distribution of W3 and W4

In order to investigate the global structure of the W3 and W4 components, we extract the amplitudes of the W3 and W4 modes in the zonal and meridional winds and temperature from the reanalysis data by using a two-dimensional least squares fit. Considering that the W2 component arises frequently in the MLT (Fritts et al., 2019), the W2 mode is also fitted together. The fitting expression is written as

$$f(\theta, t) = f_{0_j} + \sum_{j=1}^{3} A_j \sin\left(\frac{2\pi}{T}t - k_j\theta - \Phi_j\right) \quad (1)$$

where the subscript $j = 1$, 2 and 3 denotes the W2, W3, and W4 modes; θ is the longitude in units of radian; t is the time; f represents the fitted quantity, that is, the zonal wind, meridional wind and temperature, respectively; f_0 denotes the mean value of the fitted quantity; A and Φ are the amplitudes and initial phase, respectively; $T = 46$ hr is the period of the QTDW; and $k = -2$, -3 and -4 denote the zonal wavenumber of the W2, W3, and W4, respectively. The fitting window length is chosen to be 6 days with a step increment of 0.5 days. Figure 6 depicts the fitted amplitudes of the W2, W3, and W4 in the zonal and meridional winds and temperature at 0.01 hPa level (~80 km). A confidence level of 99% corresponds to the fitted amplitudes of 2.1 ms^{-1}, 2.3 ms^{-1}, and 1.2 K in the zonal wind, meridional wind and temperature, respectively. One can see the onset, enhancement and attenuation of the W3 and W4 and their latitudinal distribution at 0.01 hPa. The W3 and W4 are the predominant QTDW components in January and February, respectively. Nevertheless, the W2 can reach an amplitude of 10.4 ms^{-1} in the meridional wind over the equator on day 10, while in the zonal wind and temperature, the W2 magnitude is far smaller than the minimum values of the chosen contours, thus we will focus on the W3 and W4. The W3 increases gradually from the start of January to the maximum values in the zonal and meridional winds on about day 16 and in the temperature on day 22, and then rapidly decays and almost disappears around day about 30. At this time, the W4 grows up and attains the amplitude peak around day 35, and then fades away after day 43. Hence, the transition from the W3 to the W4 takes place in the late January and is completed around the end of January.

The latitudinal variations of the two wave modes bear much resemblance with each other. Both the W3 and W4 in the temperature have a peak value at about 45°S, and the corresponding peak amplitude is 10 K for the W3 and 6.3 K for the W4. Similarly, there is only a maximum magnitude in the meridional wind with the values of 33 ms^{-1} at 28°S for the W3 and 18.6 ms^{-1} at 35°S for the W4. As for in the zonal wind, the maximum amplitudes of both the W3 and W4 occur at the same latitude of 45°S as in the temperature, with the intensities of 24.4 and 15.1 ms^{-1}, while there is a secondary maximal peak at the same time as their maximum value, respectively. The secondary peaks of the W3 and W4 have the amplitudes of 15.3 ms^{-1} at 14°S and 10.2 ms^{-1} at 24°S, respectively, with very weak amplitudes at latitudes slightly less than 30°S. Similar latitudinal structures of the W3 in the zonal wind, meridional wind and temperature at mid latitudes of the SH are reported by Fritts et al. (2019). As shown in Figure 6, there are the two amplitude peaks in the zonal wind, we examine the phase relation between the two regions with strong wave activities. It is interesting that the phases of both the W3 and W4 are a nearly 180° out of phase with respect to about 30°S (not shown). Considering these latitudinal distributions of the wave amplitudes, the two-dimensional spectra in Figure 4 are calculated at 40°S rather than at 30°S. The wave activities are mainly concentrated in the SH, and the W3 is far stronger than the W4, thus the W3 extends much farther into the NH than the W4, which is shown in the radar observations in Figure 4.

We select a 6-day window centered on days 18 and 35 to extract the amplitudes of the two modes in the latitudinal and vertical section, respectively. Figure 7 presents the fitted amplitudes of the W3 and W4 in the zonal wind, meridional wind and temperature on days 18 and 35, and the white region means that the wave intensities are smaller than the corresponding minimum contours. The W3 and W4 have an amplitude peak in the meridional wind and temperature but two major peaks in the zonal wind in the lower mesosphere, which are consistent with those in Figure 6. The magnitude of the W3 in the temperature shows a maximal value at about 0.1 hPa level

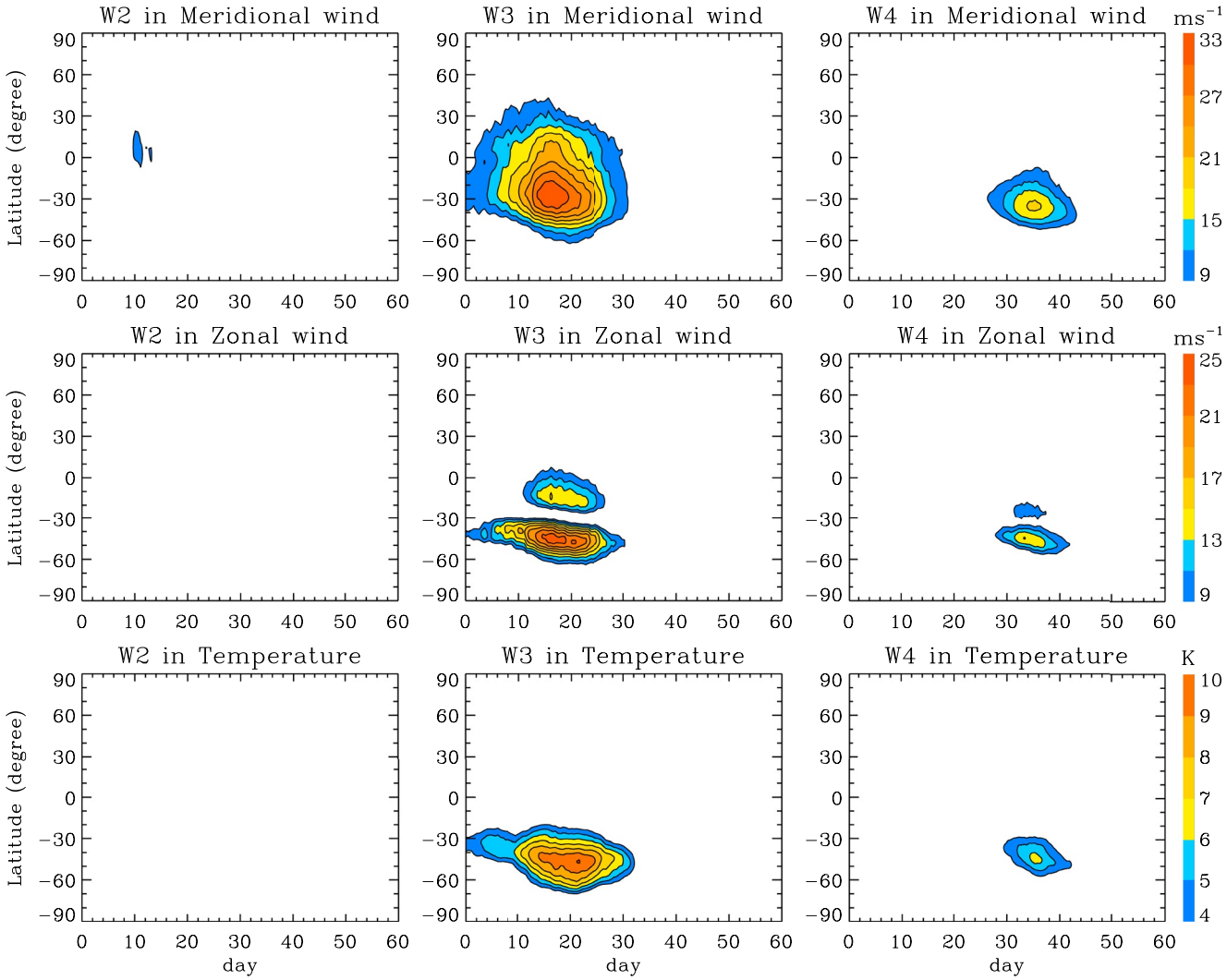

Figure 6. Temporal amplitudes of W2, W3, and W4 components in meridional wind, zonal wind, and temperature at 0.01 hPa level obtained by fitting on Modern-Era Retrospective Analysis for Research and Application version 2 reanalysis data. The left, middle, and right columns denote the amplitudes of the W2, W3, and W4, respectively.

(~64 km), and then is weakened but is subsequently strengthened with the increasing altitude. Except this, all the amplitudes of the two components in the zonal and meridional winds and temperature increase with height in the region of about 1–0.01 hPa levels (~48–80 km), and the significant QTDW activity cannot be seen below the region, implying that the main sources of both the two wave modes may be in the region of the SH. In addition, the distributions of the W3 in the zonal and meridional winds and temperature are largely consistent with the previous results in the austral solstice, but the symmetric center of the two amplitude peaks in the zonal wind is shifted to about 30°S from the near equator in the early study (Salby, 1981).

4. Wave Origination

Besides stochastic forcing, the baroclinic/barotropic instability of the summer easterly jet was proposed to be an important mechanism of QTDW excitation. In order to investigate the origination of the W3 and W4, we derived the meridional gradient of quasi-geostrophic potential vorticity ($\overline{q}_\varphi$), and the critical line and Eliassen-Palm (EP) flux of the W3 and W4 from the reanalysis data. $\overline{q}_\varphi$ is calculated from the expression as follows (Andrews et al., 1987),

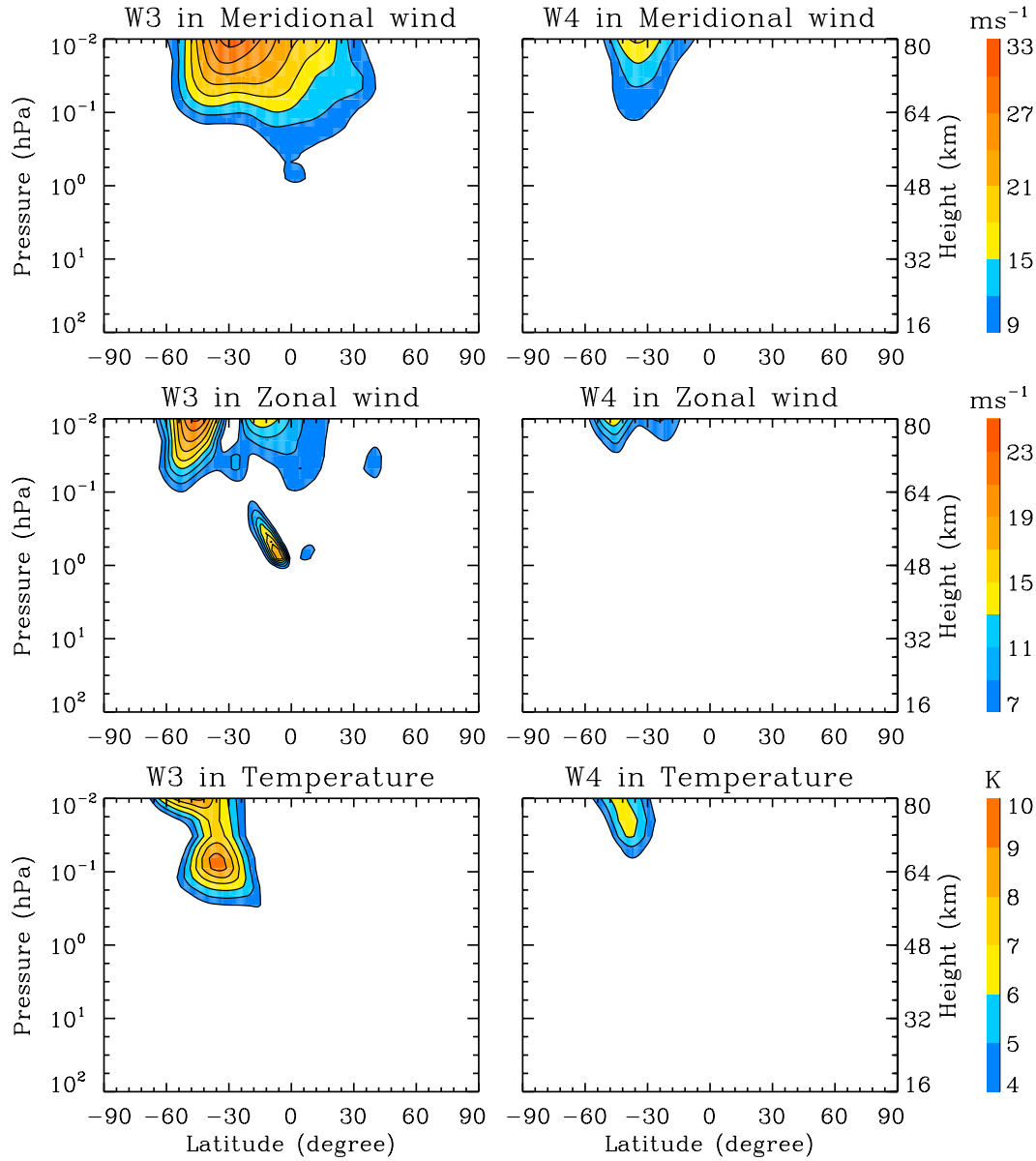

Figure 7. Fitted amplitudes of W3 centered on day 18 and W4 centered on day 35 in meridional wind, zonal wind, and temperature from Modern-Era Retrospective Analysis for Research and Application version 2 reanalysis data. The left and right columns denote the amplitudes of the W3 and W4, respectively, and the corresponding height is marked on the right vertical axis.

$$\overline{q}_{\varphi} = 2\Omega\cos\varphi - \left(\frac{\left(\overline{u}\cos\varphi\right)_{\varphi}}{a\cos\varphi}\right)_{\varphi} - \frac{a}{\rho}\left(\frac{f^2}{N^2}\rho\overline{u}_z\right)_z < 0 \tag{2}$$

where $\overline{u}$ is the zonal mean zonal wind; φ is the latitude; a is the Earth radius; Ω is the angular speed of the Earth rotation; ρ is the atmospheric density; f is the Coriolis parameter; N is the Brunt-Vaisala frequency; and the subscripts φ and z denote the derivative in the meridional and vertical directions, respectively. For the baroclinic/barotropic instability, $\overline{q}_{\varphi} < 0$ is a necessary condition (Andrews et al., 1987; Liu et al., 2004). In the critical line, the background zonal wind velocity ($\overline{u}$) equals the zonal phase velocity (c) of wave, in other words, the intrinsic frequency of wave is Doppler-shifted to zero by the background wind. If wave crosses the critical line and then moves away from the critical line, wave evanescence can occur as long as the difference ($c - \overline{u}$) between the wave

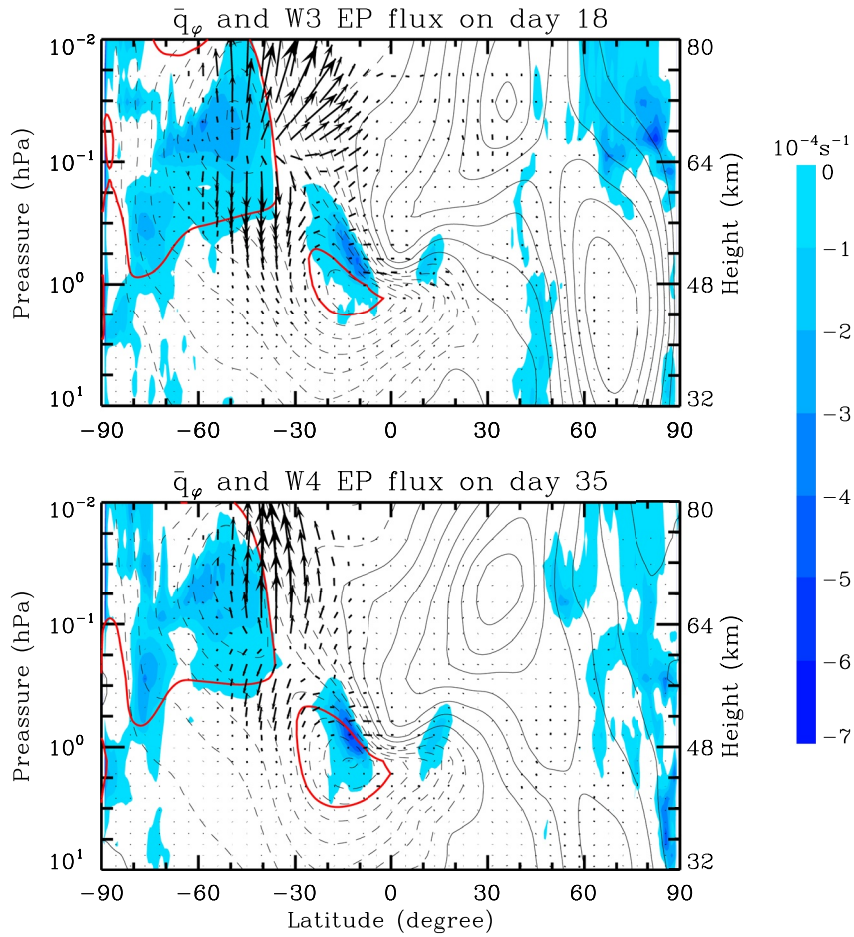

Figure 8. Meridional gradient of quasi-geostrophic potential vorticity and critical lines and Eliassen-Palm (EP) flux vectors of W3 on day 18 and W4 on day 35. The instability due to the negative meridional gradient of quasi-geostrophic potential vorticity is denoted by the blue shading. The black arrow denotes the EP flux vector, and the red curve denotes the critical line. The dashed and solid black contours denote the negative and positive zonal mean zonal winds, respectively, and the contour interval is 10 ms$-^1$. The corresponding height is marked on the right vertical axis.

phase velocity and the background wind velocity becomes large enough. When $\overline{q}_\varphi$ takes both the positive and negative values, or more strictly, satisfies $(c-\overline{u})\,\overline{q}_\varphi < 0$, the necessary condition for the baroclinic/barotropic instability is met, thus the intensity for the small amplitude perturbations may perhaps grow with time due to the possible instability (Andrews et al., 1987).

The EP flux is a physical quantity which characterizes wave-flow interaction, and its divergence represents the momentum and energy exchanges between the wave and the mean flow. The EP flux vector (**F**) and its divergence are written as (Andrews et al., 1987),

$$\mathbf{F} = (F^\varphi, F^z) = \left(-\rho a \cos\varphi \overline{v'u'}, \rho f a \cos\varphi \frac{\overline{v'\theta'}}{\overline{\theta}_z}\right) \tag{3}$$

$$\nabla \cdot \mathbf{F} = \frac{1}{a\cos\varphi}\frac{\partial}{\partial\varphi}(F^\varphi \cos\varphi) + \frac{\partial F^z}{\partial z} \tag{4}$$

where F^φ and F^z are the meridional and vertical components of the EP flux vector, respectively; u', v', and θ' are the QTDW perturbations in zonal wind, meridional wind and potential temperature, respectively, obtained from the MERRA2 data by using the two-dimensional fit in a 6-day window; and overbar denotes the zonal mean. The EP flux divergence is calculated as $(\rho a\cos\varphi)^{-1}\nabla\cdot\mathbf{F}$ in units of ms^{-1} day^{-1}, representing a coupling between the waves and the zonal-mean flow. Figure 8 shows the meridional gradient of quasi-geostrophic potential vortic-

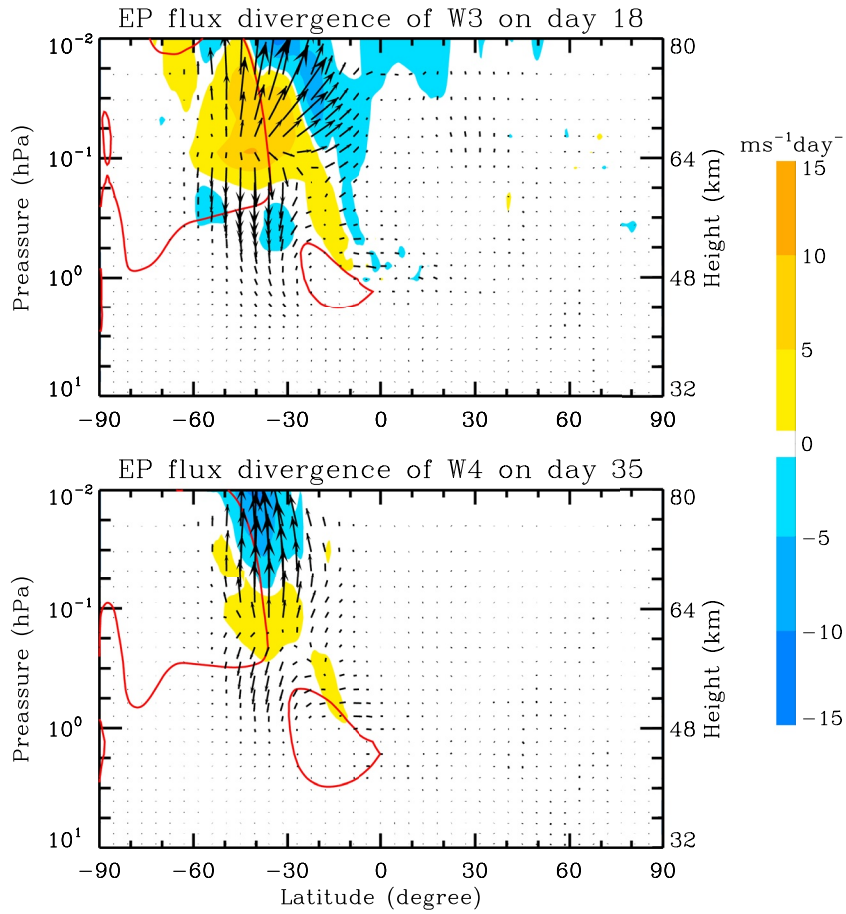

Figure 9. Eliassen-Palm (EP) flux divergences of W3 mode on day 18 and W4 mode on day 35. The color shading denotes the EP flux divergence. The black arrow denotes the EP flux vector, and the red curve denotes the critical line. The corresponding height is marked on the right vertical axis.

ity of the background atmosphere, as well as the critical lines and EP flux vectors of the W3 on day 18 and the W4 on day 35, respectively. In Figure 8, the EP flux vectors are scaled by $(p/p_0)^{-1/2}$ following Salby and Callaghan (2001) to exhibit clearly the vectors at high altitudes, and here, p is the pressure, and p_0 is the pressure on the surface. The negative values of $\overline{q}_\varphi$ are denoted with the various tones of blue to depict the possibly stronger instability. The zonal mean zonal winds and critical layers are superimposed on $\overline{q}_\varphi$ with the black contours and red curves. Figure 9 presents the EP flux divergences of the W3 on day 18 and the W4 on day 35, together with their EP flux vectors and critical lines.

During summer in the SH, there are the two easterly jet cores located at 4.76×10^{-2} hPa level (~70 km) over about 50°S and at 1.3 hPa level (~47 km) over about 12°S, respectively. On day 18, the westward wind speeds in both the two jet centers are as large as over 80 ms^{-1}. The negative $\overline{q}_\varphi$ arises around the jet centers, moreover, the critical curves in lower latitude side overlap approximately with the boundary of the unstable region, thus the essential conditions of the instability are met for the growth of small amplitude wave perturbations. Hence, it can be seen from Figures 8 and 9 that the EP flux of the W3 is generated from the unstable region and increases rapidly near the unstable region. Meanwhile, it can be noted that the region with the positive EP flux divergence is not in good agreement with the region with the negative $\overline{q}_\varphi$, which may be associated with the large amplitude wave activity and the ageostrophic and non-conservative effects in the realistic atmosphere (Andrew, 1987). Whereas, toward the polar region of the SH, the EP flux cannot be strengthened because of the strong westward wind inside the critical curves. In addition, the EP flux may transfer across the equator to the winter hemisphere, nevertheless, the strong eastward wind in the NH retards its propagation toward mid and high latitudes. In this case, the W3 in the horizontal wind and temperature has the peaks at low and mid latitudes in the SH, and is

attenuated rapidly at high latitudes of the SH due to the effect of the critical layer, and at mid and high latitudes of the NH owing to the strong eastward wind.

On day 35, the wind speeds in the two jet cores are slightly weakened. The relationship between the critical curve of the W4 and the unstable region is largely consistent with that of the W3, thus the scenarios of the EP flux and flux divergence of the W4 are similar to those of the W3. The slight difference is that the EP flux of the W4 is weaker and tends to transfer upward rather than toward low latitudes. In the numerical study (Salby & Callaghan, 2001), the W4 normal mode grows much slower than the W3 under a strong westward wind condition in January, and is more confined near the unstable region with a less global basic modal structure, which are in agreement with our results derived from the radar and reanalysis data. However, in the study of Salby and Callaghan (2001), the W3 and W4 are subjected to the numerical experiment under the same background condition in January, respectively. The response of the W3 is at a period of about 50 hr, while the rapidly amplified W4 corresponds to a period of about 41 hr much less than its theoretical value of 60 hr.

Most earlier observations indicated that the period of the W3 is generally close to 48 hr or somewhat greater, and the W4 usually has a smaller period than the W3 (Fritts et al., 1999; Harris & Vincent, 1993; Lieberman, 1999; Wu et al., 1996). In the analyses on one- and two-dimensional instability of summer easterly jets in the mesosphere, under the same background conditions, the W3 and W4 show a rapid growth in the periods of about 50 and 41 hr (Pfister, 1985; Plumb, 1983; Salby & Callaghan, 2001), respectively. Nevertheless, Plumb (1983) also suggested that the period of QTDW associated with the jet instability is dependent on the details of the jet profile. The investigation of two-dimensional jet instability demonstrated that all the jet strength, central latitude, latitudinal decay distance, vertical wind shear, and atmospheric buoyancy frequency profile have an impact on the periods of the W3 and W4 (Pfister, 1985). Besides, in the satellite measurement, the W3 has a period of about 50 hr in the NH and about 48 hr in the SH, while the W4 has a larger period of about 54 hr in both the two hemispheres (Pancheva et al., 2018). The typical periods of QTDW in the SH exhibit a regular variability from larger periods in late October to shortest periods in January, and then the periods increase in early March again, indicating that the wave period is associated with the background conditions (Pancheva et al., 2016). Hence, the 46 hr period of the W3 and W4 is slightly different from that in previous observations due possibly to the variability of background conditions.

In this study, the radar observation shows that the W3 and W4 have a nearly same dominant period of about 46 hr, which is different from earlier observations and analyses of jet instability. The equality of wave periods suggests that the two modes are subject to a similar driving process. Nonlinear interaction between QTDWs and tides was proposed to explain the rapid intensification of QTDW modes (Hecht et al., 2010; K. M. Huang, Liu, et al., 2013; Y. Y. Huang, Zhang, et al., 2013; McCormack et al., 2010; Walterscheid & Vincent, 1996), which may provide a mechanism for a joint driving process. The nearly identical period of the W3 and W4 is rarely reported in earlier studies, thus the forcing mechanisms and processes of QTDW modes require to be clarified further based on the theoretical and modeling investigation in detail.

5. Summary

In present paper, combining the observations from the four meteor radars arranged approximately along the 115°E−65°W meridian circle from the SH mid latitude to the NH mid latitude and the MERRA2 data, we study the wavenumbers 3 and 4 QTDW activities in succession in the two hemispheres.

The radar observations indicate that the QTDW activities are robust from the early January to the mid February of 2011. The QTDW in the meridional wind, with a maximum amplitude of about 80 ms^{-1}, is much stronger than in the zonal wind, and decreases gradually from mid latitudes of the SH to low and mid latitudes of the NH. The wave shows the two burst activities, and the frequency-wavenumber spectra of all the zonal and meridional winds and temperature from the reanalysis data demonstrate that the W3 dominates the first burst activity, while the W4 is the predominant component in the second burst. The W3 is more intense and lasts for a longer duration than the W4. The transition from the W3 to the W4 occurs in the late January and is completed around the end of January. Even so, the W3 and W4 have a same dominant period of about 46 hr over the two hemispheres, and the similar vertical wavelengths of about 110 km in the MLT at the Andes station of the SH and about 55–65 km in the three stations of the NH. The maximum amplitudes of both the two modes in the temperature and zonal wind are located at about 45°S, while there is a secondary maximal value only in the zonal wind at 14°S for the

W3 and at 24°S for the W4. The maximum magnitudes in the meridional wind are situated at 28°S for the W3 and 35°S for the W4, respectively.

The phases of the W3 and W4 progress downward from the MLT to the upper stratosphere. Their wave intensities grow rapidly from the upper stratosphere to the height of about 90 km, nevertheless, there are not the evident wave activities below 48 km, thus the two QTDW modes may come from the upper stratosphere and lower mesosphere, and then propagate upward to the MLT. During summer in the SH, the easterly jets at the lower mesosphere and the stratopause region have the speeds of over 80 ms^{-1}. The quasi-geostrophic potential vorticity gradients confirm the strong baroclinic/barotropic instabilities around the jet centers, and the boundaries of the unstable regions toward lower latitudes are largely consistent with the critical layers of the W3 and W4. In this case, the EP fluxes of the W3 and W4 are rapidly strengthened by the instabilities. Hence, both the W3 and W4 originate mainly from the instabilities of the jets. Besides larger magnitudes, the EP flux of the W3 shows a stronger trend of transferring across the hemispheres than that of the W4, leading to the farther extension of the W3 in the NH. The successive outbreak W3 and W4 have the nearly same period, which is rarely reported in early studies, meanwhile, this also means that the W3 and W4 are possibly subject to some additional processes, such as nonlinear energy exchanges and influences of the background conditions, which is in need of more investigation from the theory and modeling.

Data Availability Statement

Meteor radar data is accessed from the website of the IGGCAS and Chinese Meridian Project at http://wdc.geophys.ac.cn/. MERRA2 reanalysis data is accessed through the website of the NASA GES DISC at https://disc.gsfc.nasa.gov/datasets.

Acknowledgments
The authors are grateful to the editor and anonymous reviewers for their valuable comments on this paper. This work was jointly supported by the National Natural Science Foundation of China (through Grants 42174189, 41974176, and 42127805).

References

Andrews, D. G. (1987). On the interpretation of the eliassen-palm flux divergence. *Quarterly Journal of the Royal Meteorological Society*, *113*(475), 323–338. https://doi.org/10.1002/qj.49711347518

Andrews, D. G., Holton, J. R., & Leovy, C. B. (1987). *Middle atmosphere dynamics*. Elsevier.

Chang, L. C., Palo, S. E., & Liu, H. L. (2011). Short-term variability in the migrating diurnal tide caused by interactions with the quasi 2 day wave. *Journal of Geophysical Research*, *116*(D12), D12112. https://doi.org/10.1029/2010JD014996

Cheng, H., Huang, K. M., Liu, A. Z., Zhang, S. D., Huang, C. M., & Gong, Y. (2021). A quasi-27-day oscillation activity from the troposphere to the mesosphere and lower thermosphere at low latitudes. *Earth Planets and Space*, *73*(1), 183. https://doi.org/10.1186/s40623-021-01521-1

Craig, R. L., Vincent, R. A., Fraser, G. J., & Smith, M. J. (1980). The quasi 2-day wave in the Southern Hemisphere mesosphere. *Nature*, *287*(5780), 319–320. https://doi.org/10.1038/287319a0

Ern, M., Preusse, P., Kalisch, S., Kaufmann, M., & Riese, M. (2013). Role of gravity waves in the forcing of quasi two-day waves in the mesosphere: An observational study. *Journal of Geophysical Research: Atmospheres*, *118*(9), 3467–3485. https://doi.org/10.1029/2012JD018208

Forbes, J. M., & Moudden, Y. (2012). Quasi-two-day wave-tide interactions as revealed in satellite observations. *Journal of Geophysical Research*, *117*(D12), D12110. https://doi.org/10.1029/2011JD017114

Franke, S. J., Chu, X., Liu, A. Z., & Hocking, W. K. (2005). Comparison of meteor radar and Na Doppler lidar measurements of winds in the mesopause region above Maui, Hawaii. *Journal of Geophysical Research*, *110*(D9), D09S02. https://doi.org/10.1029/2003JD004486

Fritts, D. C., Iimura, H., Janches, D., Lieberman, R. S., Riggin, D. M., Mitchell, N. J., et al. (2019). Structure, variability, and mean-flow interactions of the January 2015 quasi-2-day wave at middle and high southern latitudes. *Journal of Geophysical Research: Atmospheres*, *124*(12), 5981–6008. https://doi.org/10.1029/2018JD029728

Fritts, D. C., Isler, J. R., Lieberman, R. S., Burrage, M. D., Marsh, D. R., Nakamura, T., et al. (1999). Two-day wave structure and mean flow interactions observed by radar and High Resolution Doppler Imager. *Journal of Geophysical Research*, *104*(D4), 3953–3969. https://doi.org/10.1029/1998JD200024

Gaikwad, H. P., Sharma, A. K., Gurav, O. B., Chavan, G. A., Nade, D. P., Patil, P. T., et al. (2019). Seasonal, annual, and interannual variability in MLT quasi-two-day waves over the low-latitude region Kolhapur (16.8°N; 74.2°E). *Advances in Space Research*, *63*(7), 2100–2117. https://doi.org/10.1016/j.asr.2018.12.029

Garcia, R. R., Lieberman, R., Russell, J. M., III, & Mlynczak, M. G. (2005). Large-scale waves in the mesosphere and lower thermosphere observed by SABER. *Journal of the Atmospheric Sciences*, *62*(12), 4384–4399. https://doi.org/10.1175/JAS3612.1

Gelaro, R., McCarty, W., Suárez, M. J., Todling, R., Molod, A., Takacs, L., et al. (2017). The modern-era retrospective analysis for research and applications, version 2 (MERRA-2). *Journal of Climate*, *30*(14), 5419–5454. https://doi.org/10.1175/JCLI-D-16-0758.1

Gu, S. Y., Li, T., Dou, X., Wu, Q., Mlynczak, M. G., & Russell, J. M., III. (2013). Observations of quasi-two-day wave by TIMED/SABER and TIMED/TIDI. *Journal of Geophysical Research: Atmospheres*, *118*(4), 1624–1639. https://doi.org/10.1002/jgrd.50191

Hagan, M. E., Forbes, J. M., & Vial, F. (1993). Numerical investigation of the propagation of the quasi-two-day wave into the lower thermosphere. *Journal of Geophysical Research*, *98*(D12), 23193–23205. https://doi.org/10.1029/93JD02779

Harris, T. J., & Vincent, R. A. (1993). The quasi-two-day wave observed in the equatorial middle atmosphere. *Journal of Geophysical Research*, *98*(D6), 10481–10490. https://doi.org/10.1029/93JD00380

He, M., Chau, J. L., Forbes, J. M., Zhang, X., Englert, C. R., Harding, B. J., et al. (2021). Quasi-2-day wave in low-latitude atmospheric winds as viewed from the ground and space during January–March, 2020. *Geophysical Research Letters*, *48*(13), e2021GL093466. https://doi.org/10.1029/2021GL093466

He, M., Forbes, J. M., Li, G., Jacobi, C., & Hoffmann, P. (2021). Mesospheric Q2DW interactions with four migrating tides at 53°N latitude: Zonal wavenumber identification through dual-station approaches. *Geophysical Research Letters*, *48*(8), e2020GL092237. https://doi.org/10.1029/2020GL092237

Hetch, J. H., Walterscheid, R. L., Gelinas, L. J., Vincent, R. A., Reid, I. M., & Woithe, J. M. (2010). Observations of the phase-locked 2 day wave over the Australian sector using medium-frequency radar and airglow data. *Journal of Geophysical Research*, *115*(D16), D16115. https://doi.org/10.1029/2009JD013772

Hocking, W. K., Fuller, B., & Vandepeer, B. (2001). Real-time determination of meteor-related parameters utilizing modern digital technology. *Journal of Atmospheric and Solar-Terrestrial Physics*, *63*(2–3), 155–169. https://doi.org/10.1016/S1364-6826(00)00138-3

Huang, K. M., Liu, A. Z., Lu, X., Li, Z., Gan, Q., Gong, Y., et al. (2013). Nonlinear coupling between quasi 2 day wave and tides based on meteor radar observations at Maui. *Journal of Geophysical Research: Atmospheres*, *118*(19), 10936–10943. https://doi.org/10.1002/jgrd.50872

Huang, K. M., Liu, A. Z., Zhang, S. D., Yi, F., Huang, C. M., Gan, Q., et al. (2015). Observational evidence of quasi-27-day oscillation propagating from the lower atmosphere to the mesosphere over 20°N. *Annales Geophysicae*, *33*(10), 1321–1330. https://doi.org/10.5194/angeo-33-1321-2015

Huang, K. M., Xi, Y., Wang, R., Zhang, S. D., Huang, C. M., Gong, Y., & Cheng, H. (2019). Signature of a quasi 30-day oscillation at midlatitude based on wind observations from MST radar and meteor radar. *Journal of Geophysical Research: Atmospheres*, *124*(21), 11266–11280. https://doi.org/10.1029/2019JD031170

Huang, X. S., Huang, K. M., Zhang, S. D., Huang, C. M., Gong, Y., & Cheng, H. (2022). Extraordinary quasi-16-day wave activity from October 2013 to January 2014 with radar observations at mid-latitudes and MERRA2 reanalysis data. *Earth Planets and Space*, *74*(1), 98. https://doi.org/10.1186/s40623-022-01660-z

Huang, Y. Y., Zhang, S. D., Yi, F., Huang, C. M., Huang, K. M., Gan, Q., & Gong, Y. (2013). Global climatological variability of quasi-two-day waves revealed by TIMED/SABER observations. *Annales Geophysicae*, *31*(6), 1061–1075. https://doi.org/10.5194/angeo-31-1061-2013

Jacobi, C., Schminder, R., & Kürschner, D. (1997). The quasi 2-day wave as seen from D1 LF wind measurements over central Europe (52°N, 15°E) at Collm. *Journal of Atmospheric and Solar-Terrestrial Physics*, *59*(11), 1277–1286. https://doi.org/10.1016/S1364-6826(96)00170-8

Jacobi, C., Schminder, R., & Kürschner, D. (1998). Non-linear interaction of the quasi 2-day wave and long-term oscillations in the summer midlatitude mesopause region as seen from LF D1 wind measurements over Central Europe (Collm, 52°N, 15°E). *Journal of Atmospheric and Solar-Terrestrial Physics*, *60*(12), 1175–1191. https://doi.org/10.1016/S1364-6826(98)00076-5

Lieberman, R. S. (1999). Eliassen-Palm fluxes of the 2-day wave. *Journal of the Atmospheric Sciences*, *56*(16), 2846–2861. https://doi.org/10.1175/1520-0469(1999)056<2846:EPFOTD>2.0.CO;2

Lilienthal, F., & Jacobi, C. (2015). Meteor radar quasi 2-day wave observations over 10 years at Collm (51.3°N, 13.0°E). *Atmospheric Chemistry and Physics*, *15*(17), 9917–9927. https://doi.org/10.5194/acp-15-9917-2015

Lima, L. M., Batista, P. P., Takahashi, H., & Clemesha, B. R. (2004). Quasi-two-day wave observed by meteor radar at 22.7°S. *Journal of Atmospheric and Solar-Terrestrial Physics*, *66*(6–9), 529–537. https://doi.org/10.1016/j.jastp.2004.01.007

Limpasuvan, V., & Wu, D. L. (2003). Two-day wave observations of UARS Microwave Limb Sounder mesospheric water vapor and temperature. *Journal of Geophysical Research*, *108*(D10), 4307. https://doi.org/10.1029/2002JD002903

Limpasuvan, V., & Wu, D. L. (2009). Anomalous two-day wave behavior during the 2006 austral summer. *Geophysical Research Letters*, *36*(4), L04807. https://doi.org/10.1029/2008GL036387

Liu, H. L., Talaat, E. R., Roble, R. G., Lieberman, R. S., Riggin, D. M., & Yee, J. H. (2004). The 6.5-day wave and its seasonal variability in the middle and upper atmosphere. *Journal of Geophysical Research*, *109*(D21), D21112. https://doi.org/10.1029/2004JD004795

Malinga, S. B., & Ruohoniemi, J. M. (2007). The quasi-two-day wave studied using the Northern Hemisphere SuperDARN HF radars. *Annales Geophysicae*, *25*(8), 1767–1778. https://doi.org/10.5194/angeo-25-1767-2007

Manney, G. L., Daffer, W. H., Strawbridge, K. B., Walker, K. A., Boone, C. D., Bernath, P. F., et al. (2008). The high arctic in extreme winters: Vortex, temperature, and MLS and ACE-FTS trace gas evolution. *Atmospheric Chemistry and Physics*, *8*(3), 505–522. https://doi.org/10.5194/acp-8-505-2008

McCormack, J. P., Coy, L., & Hoppel, K. W. (2009). Evolution of the quasi 2-day wave during January 2006. *Journal of Geophysical Research*, *114*(D20), D20115. https://doi.org/10.1029/2009JD012239

McCormack, J. P., Eckermann, S. D., Hoppel, K. W., & Vincent, R. A. (2010). Amplification of the quasi-two day wave through nonlinear interaction with the migrating diurnal tide. *Geophysical Research Letters*, *37*(16), L16810. https://doi.org/10.1029/2010GL043906

Moudden, Y., & Forbes, J. M. (2014). Quasi-two-day wave structure, interannual variability, and tidal interactions during the 2002–2011 decade. *Journal of Geophysical Research: Atmospheres*, *119*(5), 2241–2260. https://doi.org/10.1002/2013JD020563

Norton, W. A., & Thuburn, J. (1996). The two-day wave in a middle atmosphere GCM. *Geophysical Research Letters*, *23*(16), 2113–2116. https://doi.org/10.1029/96GL01956

Palo, S. E., Forbes, J. M., Zhang, X., Russell, J. M., III, & Mlynczak, M. G. (2007). An eastward propagating two-day wave: Evidence for nonlinear planetary wave and tidal coupling in the mesosphere and lower thermosphere. *Geophysical Research Letters*, *34*(7), L07807. https://doi.org/10.1029/2006GL027728

Palo, S. E., Roble, R. G., & Hagan, M. E. (1999). Middle atmosphere effects of the quasi-two-day wave determined from a General Circulation Model. *Earth Planets and Space*, *51*(7–8), 629–647. https://doi.org/10.1186/BF03353221

Pancheva, D., Mitchell, N. J., Manson, A. H., Meek, C. E., Jacobi, C., Portnyagin, Y., et al. (2004). Variability of the quasi-2-day wave observed in the MLT region during the PSMOS campaign of June-August 1999. *Journal of Atmospheric and Solar-Terrestrial Physics*, *66*(6–9), 539–565. https://doi.org/10.1016/j.jastp.2004.01.008

Pancheva, D., Mukhtarov, P., & Siskind, D. E. (2018). Climatology of the quasi-2-day waves observed in the MLS/Aura measurements (2005–2014). *Journal of Atmospheric and Solar-Terrestrial Physics*, *171*, 210–224. https://doi.org/10.1016/j.jastp.2017.05.002

Pancheva, D., Mukhtarov, P., Siskind, D. E., & Smith, A. K. (2016). Global distribution and variability of quasi 2 day waves based on the NOGAPS-ALPHA reanalysis model. *Journal of Geophysical Research: Space Physics*, *121*(11), 11422–11449. https://doi.org/10.1002/2016JA023381

Pfister, L. (1985). Baroclinic instability of easterly jets with applications to the summer mesosphere. *Journal of the Atmospheric Sciences*, *42*(4), 313–330. https://doi.org/10.1175/1520-0469(1985)042<0313:BIOEJW>2.0.CO;2

Plumb, R. A. (1983). Baroclinic instability of the summer mesosphere: A mechanism for the quasi-two-day wave? *Journal of the Atmospheric Sciences*, *40*(1), 262–270. https://doi.org/10.1175/1520-0469(1983)040<0262:BIOTSM>2.0.CO;2

Rao, N. V., Ratnam, M. V., Vedavathi, C., Tsuda, T., Murthy, B. V. K., Sathishkumar, S., et al. (2017). Seasonal, inter-annual and solar cycle variability of the quasi two day wave in the low-latitude mesosphere and lower thermosphere. *Journal of Atmospheric and Solar-Terrestrial Physics*, *152–153*, 20–29. https://doi.org/10.1016/j.jastp.2016.11.005

Richter, J. H., Sassi, F., Garcia, R. R., Matthes, K., & Fischer, C. A. (2008). Dynamics of the middle atmosphere as simulated by the whole atmosphere community climate model, version 3 (WACCM3). *Journal of Geophysical Research*, *113*(D8), D08101. https://doi.org/10.1029/2007JD009269

Riggin, D. M., Lieberman, R. S., Vincent, R. A., Manson, A. H., Meek, C. E., Nakamura, T., et al. (2004). The 2-day wave during the boreal summer of 1994. *Journal of Geophysical Research*, *109*(D8), D08110. https://doi.org/10.1029/2003JD004493

Salby, M. L. (1981). The 2-day wave in the middle atmosphere: Observations and theory. *Journal of Geophysical Research*, *86*(C10), 9654–9660. https://doi.org/10.1029/JC086iC10p09654

Salby, M. L. (1984). Survey of planetary-scale traveling waves: The state of theory and observations. *Reviews of Geophysics*, *22*(2), 209–236. https://doi.org/10.1029/RG022i002p00209

Salby, M. L., & Callaghan, P. F. (2001). Seasonal amplification of the 2-day wave: Relationship between normal mode and instability. *Journal of the Atmospheric Sciences*, *58*(14), 1858–1869. https://doi.org/10.1175/1520-0469(2001)058<1858:SAOTDW>2.0.CO;2

Schröder, H., & Schmitz, G. (2004). A generation mechanism for the 2-day wave near the stratopause: Mixed barotropic-inertial instability. *Journal of Geophysical Research*, *109*(D24), D24116. https://doi.org/10.1029/2004JD005177

Suresh Babu, V., Kishore Kumar, K., John, S. R., Subrahmanyam, K. V., & Ramkumar, G. (2011). Meteor radar observations of short-term variability of quasi 2 day waves and their interaction with tides and planetary waves in the mesosphere-lower thermosphere region over Thumba (8.5°N, 77°E). *Journal of Geophysical Research*, *116*(D16), D16121. https://doi.org/10.1029/2010JD015390

Thayaparan, T., Hocking, W. K., MacDougall, J., Manson, A. H., & Meek, C. E. (1997). Simultaneous observations of the 2-day wave at London (43°N, 81°W) and Saskatoon (52°N, 107°W) near 91°km altitude during the two years of 1993 and 1994. *Annales Geophysicae*, *15*(10), 1324–1339. https://doi.org/10.1007/s00585-997-1324-3

Tsuda, T., Kato, S., & Vincent, R. A. (1988). Long period wind oscillations observed by the Kyoto meteor radar and comparison of the quasi-2-day wave with Adelaide HF radar observations. *Journal of Atmospheric and Terrestrial Physics*, *50*(3), 225–230. https://doi.org/10.1016/0021-9169(88)90071-2

Tunbridge, V. M., Sandford, D. J., & Mitchell, N. J. (2011). Zonal wave numbers of the summertime 2 day planetary wave observed in the mesosphere by EOS Aura Microwave Limb Sounder. *Journal of Geophysical Research*, *116*(D11), D11103. https://doi.org/10.1029/2010JD014567

Walterscheid, R. L., & Vincent, R. A. (1996). Tidal generation of the phase-locked 2-day wave in the southern hemisphere summer by wave-wave interactions. *Journal of Geophysical Research*, *101*(D21), 26567–26576. https://doi.org/10.1029/96JD02248

Wu, D. L., Fishbein, E. F., Read, W. G., & Waters, J. W. (1996). Excitation and evolution of the quasi-2-day wave observed in UARS/MLS temperature measurements. *Journal of the Atmospheric Sciences*, *53*(5), 728–738. https://doi.org/10.1175/1520-0469(1996)053<0728:EAEOTQ>2.0.CO;2

Yu, F. R., Huang, K. M., Zhang, S. D., Huang, C. M., Yi, F., Gong, Y., et al. (2019). Quasi 10- and 16-day wave activities observed through meteor radar and MST radar during stratospheric final warming in 2015 spring. *Journal of Geophysical Research: Atmospheres*, *124*(12), 6040–6056. https://doi.org/10.1029/2019JD030630

Yu, Y., Wan, W., Ren, Z., Xiong, B., Zhang, Y., Hu, L., et al. (2015). Seasonal variations of MLT tides revealed by a meteor radar chain based on Hough mode decomposition. *Journal of Geophysical Research: Space Physics*, *120*(8), 7030–7048. https://doi.org/10.1002/2015JA021276

Yue, J., Liu, H. L., & Chang, L. C. (2012). Numerical investigation of the quasi 2 day wave in the mesosphere and lower thermosphere. *Journal of Geophysical Research*, *117*(D5), D05111. https://doi.org/10.1029/2011JD016574